Aerodynamics for MDO of an innovative configuration

G. Bernardini, A. Frediani
Dipartimento di Ingegneria Aerospaziale
Università degli Studi di Pisa
Via Diotisalvi 2, 56126 Pisa, Italy

L. Morino
Dipartimento di Ingegneria Meccanica e Industriale
Università degli Studi *Roma Tre*
Via della Vasca Navale 79, 00146 Roma, Italy

Abstract

A numerical methodology for the evaluation of aerodynamic loads acting on a complex lifting configuration is presented. The work is limited to the case of attached high-Reynolds number flows. A viscous/potential interaction technique is utilized to take into account the effects of the viscosity. For the potential-flow analysis, a boundary element formulation is used; for simplicity, only incompressible flows are examined. The theoretical basis of the present methodology is briefly described. Comparisons with available, numerical and experimental results are included.

1. Introduction

The present work is an overview paper on recent results on viscous–flow analysis of innovative configurations (low–induced drag lifting configurations), obtained by the authors within the objective of developing an MDO methodology. The aerodynamic methodology is based on a boundary element formulation for the velocity potential introduced by Morino [16]; the effects of viscosity are taken into account by a classical viscous/inviscid coupling technique; a technique for extending this approach beyond the limits of the boundary–layer approach is also indicated.

In order to put this work in the paper context, note that, the increased request for low–cost air transportation has generated considerable interest for non–conventional configurations, such as biplanes with wing tips connected to each other directly (joined wing configuration) or through a vertical surface (box–wing configuration). These configurations are related to the early work of Prandtl [25] on multiplanes, which shows that these configurations have certain aerodynamic advantages (outlined in the following sentences) with respect to isolated wings. First, the induced drag of a multiplane with elliptic distribution of circulation is lower than the induced drag of the equivalent monoplane (*i.e.*, of the monoplane having the same span and generating the same lift as the multiplane considered). In addition, the ratio, K, between the induced drag of a multiplane and that of the equivalent monoplane, decreases as the number of wings of the multiplane increases (with global height and lift kept constant). In the limit as the number of wings tends to infinity ("infinity–plane", according to the Prandtl [25] definition), K has the minimum value. Finally, there exists a box–wing type configuration that has the same distribution of circulation (and hence the same K) as the "infinity–plane"; such configuration is therefore designated, still by Prandtl [25], at the 'Best Wing System' (BWS).

After the work of Prandtl [25], valid only for the limited case of multiplanes with elliptic distribution of circulation, several numerical and experimental studies have been published. Of particular interest here is, the work of Nenadovitch [23] on the efficiency of bidimensional biplanes. Also, an experimental analysis of joined wing aircraft is presented by Wolkovitch [32], whereas experimental as well as numerical/empirical studies on biplanes and box–wing configurations are proposed by Gall and Smith [6].

In this paper, the attention is focused on an innovative configuration for a new large dimension aircraft (usually indicated as New Large Airplanes or NLA)

Paper presented at the RTO AVT Symposium on "Aerodynamic Design and Optimisation of Flight Vehicles in a Concurrent Multi-Disciplinary Environment", held in Ottawa, Canada, 18-21 October 1999, and published in RTO MP-35.

proposed by Frediani *et al.* [4], [5]. This configuration is a biplane, with counter–swept wings (positive sweep for the front lower wing and negative sweep for the back upper wing, which acts as a horizontal tail as well) connected to each other by aerodynamic surfaces (Figures 1 and 2). Following Frediani *et al.* [4], [5] we will refer to this configuration as the Prandtl–plane. Preliminary numerical and experimental studies (Frediani *et al.* [4], [5]) have shown that the induced drag of this configuration is lower than the induced drag of an equivalent monoplane. This fact allows one to reduce the wingspan of this configuration without drag penalties and introduces the possibility of respecting the maximum span–wise dimensions (critical for the NLA with classical wing configuration), which would allow compatibility with the existing airport regulations.

Still to in order to put the work in the paper context, note that through an unrelated activity, the authors have been involved in the developement of an MDO code. The weakest module in this code is the aerodynamic one. In fact, the aerodynamic module in such a code is limited to potential flows around simply–connected domains; on the contrary, the Prandtl–plane configuration is multiply–connected. In addition, a key for this configurations (and MDO in general) is the drag, induced and viscous.

These issues are addressed in this paper, as a first step towards generating a suitable viscous aerodynamic module around multiply–connected configurations, to be incorporated in the above mentioned MDO code. Specifically, because of the complexity and novelty of the configurations discussed above, it is desirable to develop an aerodynamic methodology for multiply–connected configurations capable of yielding accurate predictions with a relatively small computational effort (hence, not a CFD approach), which takes into account the effects of viscosity and of the wake roll–up (the geometry of the rolled–up wake is evaluated through the free–wake analysis of Ref. [29]). The relatively recent state of our work in this context was presented in Bernardini *et al.* [1], which is based on the classical viscous–potential interaction, with the viscous flow (in boundary layer and wake) solved by using the strip–theory approach, with an integral two–dimensional boundary layer; the viscous/inviscid coupling technique is based upon the Lighthill [12] equivalent–sources approach. Matching of the boundary–layer solution with the corrected potential–flow solution is obtained by direct iteration. Here, the emphasis is on the most recent improvements with respect to that paper. First, we present an extension to higher order of the direct boundary element formulation used in the past by the authors for incompressible potential flows around lifting objects of arbitrary shape in uniform translation; this provides also an opportunity to clarify certain theoretical issues connected with the trailing edge conditions. Second, we discuss a three–dimensional integral boundary–layer formulation, which is based essentially on the algorithm of Nishida [24] and Milewski [15]. The solution is obtained through the simultaneous coupling technique introduced by Drela [3].

2. Formulation of Ref. [1]

The formulation of Bernardini *et al.* [1] is outlined here in order to emphasize the differences of the new formulation and also because, some new results presented here are based on this formulation. For a detailed discussion, see Ref. [18], where a review is also presented.

Potential–Flow Formulation: an inviscid, incompressible, initially–irrotational flow remains at all times quasi–potential (*i.e.*, potential everywhere except for the wake surface, which is the locus of the points emanating from the trailing–edge). In this case, the velocity field, $\mathbf{v}$, may be expressed as $\mathbf{v} = \nabla\varphi$ (where φ is the velocity potential). Combining with the continuity equation for incompressible flows, $\nabla \cdot \mathbf{v} = 0$,

yields

$$\nabla^2\varphi = 0. \tag{1}$$

The boundary conditions for this equation are as follows. The surface of the body, $\mathcal{S}_B$, is assumed to be impermeable; this yields $(\mathbf{v} - \mathbf{v}_B)\cdot\mathbf{n} = 0$, *i.e.*,

$$\frac{\partial\varphi}{\partial n} = \mathbf{v}_B\cdot\mathbf{n} \qquad \text{for } \mathbf{x}\in\mathcal{S}_B, \tag{2}$$

where $\mathbf{v}_B$ is the velocity of a point $\mathbf{x}\in\mathcal{S}_B$, whereas $\mathbf{n}$ is the outward unit normal to $\mathcal{S}_B$. At infinity, in a frame of reference fixed with the unperturbed fluid, we have $\varphi = 0$. The boundary condition on the wake surface, $\mathcal{S}_W$, are: *(i)* the wake surface is impermeable, and *(ii)* the pressure, p, is continuous across it. These imply that $\Delta(\partial\varphi/\partial n) = 0$ (where Δ denotes discontinuity across $\mathcal{S}_W$), and that $\Delta\varphi$ remains constant in time following a wake point $\mathbf{x}_W$ (whose velocity is the average of the fluid velocity on the two sides of the wake), and equals the value it had when $\mathbf{x}_W$ left the trailing edge. This value is obtained by imposing the trailing-edge condition that, at the trailing edge, $\Delta\varphi$ on the wake equals $\varphi_u - \varphi_l$ on the body (subscripts u and l denote, respectively, upper and lower sides of the body surface).

In this paper, the above problem for the velocity potential is solved by a boundary element formulation. The boundary integral representation for the above problem is given by

$$\begin{aligned}\varphi(\mathbf{x}) &= \int_{\mathcal{S}_B}\left(G\chi - \varphi\frac{\partial G}{\partial n}\right)d\mathcal{S}(\mathbf{y}) \\ &- \int_{\mathcal{S}_W}\Delta\varphi\frac{\partial G}{\partial n}d\mathcal{S}(\mathbf{y}),\end{aligned} \tag{3}$$

with $\chi := \mathbf{v}_B\cdot\mathbf{n}$, and $G = -1/4\pi\|\mathbf{y}-\mathbf{x}\|$. Note that, in the absence of the wake, Eq. 3, in the limit as $\mathbf{x}$ tends to $\mathcal{S}_B$, represents a boundary integral equation for φ on $\mathcal{S}_B$, with χ on $\mathcal{S}_B$ known from the boundary condition. Once φ on the body is known, φ (and hence $\mathbf{v}$ and, by using Bernoulli's theorem, p) may be evaluated everywhere in the field. The situation is similar in the presence of the wake, since, by applying the wake and trailing–edge conditions, $\Delta\varphi$ on the wake may be expressed in terms of φ over the body at preceding times.

In Bernardini *et al.* [1], the boundary integral equation for φ based on Eq. 3 is solved numerically by discretizing the body and wake surfaces in quadrilateral elements, assuming φ, χ and $\Delta\varphi$ to be piecewise constant, and imposing that the equation be satisfied at the center of each body element (zeroth–order boundary–element collocation method).

It should be noted that the geometry of the wake is not known *a priori*. For the case of isolated wings in uniform translation, a flat wake with vortical lines parallel to the unperturbed streamlines is typically used (prescribed–wake analysis). In the configuration of interest here, such *a priori* assumptions are not justified by past experience. Still in Bernardini *et al.* [1], the wake geometry is either prescribed (undisturbed) or obtained through a free–wake analysis, *i.e.*, the boundary integral equation is used to compute, at each time step t_n the flow velocity at nodes $\mathbf{x}_i$ of the discretized wake surface (free–wake analysis); the locations of $\mathbf{x}_i$ at t_{n+1} is then obtained by integrating the equation $\dot{\mathbf{x}}_i = \mathbf{v}_i(\mathbf{x}_p)$ by the explicit Euler method (in other words, in the case of free–wake analysis the shape of the wake and the flowfield solution are obtained step–by–step, as part of the solution). For the steady–state cases of interest here, the solution is obtained in the limit as the solution for $t\to\infty$ of a transient flow due to an impulsive start. Incidentally, this procedure resolves also the non–uniquess issue connected with steady–state flows around multiply–connected region; indeed, in the case of unsteady flow the solution is unique, because Kelvin's theorem allows one to obtain the circulation on the wing from the vorticity shed in the wake (see Ref. [20]).

Boundary Layer: the viscous flow analysis is limited to attached steady high–Reynolds number flows. Under these assumptions, a classical integral boundary–layer formulation may be used. Specifically, Bernar-

dini *et al.* [1] use a 2D integral boundary–layer formulation used as 'strip–theory'. The laminar portion is computed by using the Thwaites collocation method [30]. The transition from laminar to turbulent flow is detected by the Michel method [14]. The turbulent portion of the boundary layer and wake are studied by the 'lag-entrainment' method of Green *et al.* [9].

Viscous/Inviscid Coupling: once the boundary–layer equations are solved, the viscous correction to the potential flow is obtained as a transpiration velocity through $\mathcal{S}_B$ and $\mathcal{S}_W$ (equivalent source method by Lighthill [12]). The boundary condition for φ over the body surface is modified as follows

$$\partial\varphi/\partial n = \mathbf{v}_B \cdot \mathbf{n} + \chi_V,$$

where the transpiration velocity χ_V is given by

$$\chi_V = \frac{\partial}{\partial s}(u_e \delta^*) = \frac{\partial}{\partial s}\int_0^\delta (u_e - u)\, dz, \qquad (4)$$

where s denotes the arclength in the 2D boundary–layer and wake, and δ^* is the displacement thickness. In addition, u and u_e denote, respectively, the velocity within the vortical layer and at its outer edge (in a frame of reference fixed with the body). On the wake surface one has

$$\Delta(\partial\varphi/\partial n) = (\chi_V)_u + (\chi_V)_l,$$

where the subscripts u and l denote, respectively, the upper and lower sides of the wake surface.

3. Third–order extension

The specific formulation used here is based upon a high–order formulation introduced by Gennaretti *et al.* [8], and extended in Refs. [20] and [21], to which the reader is referred for details (here the emphasis is on the applications). This consists of using bicubic quadrilateral elements and the Hermite interpolation for φ in both directions. This yields a bicubic representation in terms of the nodal values of φ, $\partial\varphi/\partial\xi$, $\partial\varphi/\partial\eta$, and $\partial^2\varphi/\partial\xi\partial\eta$; the nodal derivatives are then expressed in terms of the unknowns of the problem, φ_i, through suitable finite–difference approximations. Only steady flows are considered here; then, the wake geometry at the trailing–edge (typically tangents to one of the sides of the body surface at the trailing–edge) may be determined by the results of Mangler and Smith [13].

The above formulation generates new issues connected to the trailing–edge. The first one, is related to the existence of the trailing–edge potential discontinuity which implies that at any trailing–edge node there exist two unknowns, but only one collocation point. Gennaretti *et al.* [8] use two collocation points suitably located slightly ahead of the trailing edge (otherwise the collocation points coincide with the nodes).

In order to avoid ill–conditioned matrix here, as mentioned above, we use the approach introduced in Ref. [20], who, at the trailing–edge, use only one control point but two different integral equations: the first is the potential equation while the second is its derivative in the direction of the wake normal at trailing–edge.

An additional issue stemming from the third–order formulation is that of the evaluation of the derivatives of φ at the trailing edge. These may be obtained by imposing the two conditions of stagnation point and smooth flow (see Ref. [20] for details).

4. Three–dimensional boundary layer

In order to take into account the three–dimensional effects, the viscous flow in the boundary layer and wake, is modelled using the three-dimensional integral boundary–layer equations on non–ortogonal grids. Specifically, the integral method uses two equations for momentum (extention of von Kármán equation to 3D flows) coupled by two auxiliary equations. The first is the kinetic energy equation and the second is the transport equation for the maximum shear stess coefficient ('lag' equation). In order to complete the problem, we use, following Nishida [24] and Milewski [15], the streamwise closure relations pro-

posed by Drela [3] in his 2D integral boundary–layer method, along with the crosswise relations of Johnston [11]. The Mughal [22] finite–volume scheme is used for the solution.

Also in this case, the viscosity correction to the potential flow is evaluated as a transpiration velocity through $\mathcal{S}_B$ and $\mathcal{S}_W$ (equivalent source method by Lighthill [12]). However, as mentioned above, in contrast with the formulation of Bernardini *et al.* [1], the matching of the thin–layer solution with the potential–flow solution, is obtained by the fully simultaneous coupling method of Drela [3], which solves the viscous and inviscid equations simultaneously and is stable even for separated flows.

5. Numerical results and comments

The results presented here fall into three groups. In the first group are some new results obtained with the formulation outlined in Section 2 (some of the results of Ref. [1] are included here for the sake of clarity). The second and third group are based on the formulations of Sections 3 and 4.

For all the potential flow results, the airloads are determined by using the formulation of Ref. [7], which is an exact generalization of the Trefftz–plane theory [31] for the evaluation of aerodynamic loads around objects of arbitrary shapes. The viscous drag is evaluated by using the classical formula by Squire and Young [28].

First, a few results obtained by Bernardini *et al.* [1] are discussed as they help in putting the paper in the proper context. First of all, the potential flow formulation of Section 2 has been validated in Ref. [1] by a comparison with analytical results by Prandtl [25] either in the case of biplanes and box–wing configuration; this comparison has shown nearly perfect agreement between our numerical results and the analytical results of Prandtl. Also, in order to analyze the mechanism of induced–drag reduction, it is interesting to compare the efficiency K of: *(i)* a rectangular biplane; *(ii)* a rectangular biplane with facing tip winglets on the two wings and *(iii)* a box–wing. For, this show the graduality of the reduction (in the sense that the biplane corresponds to the zero winglet–length case and the wing–box to the full length case); this is apparent from Figure 3 (from Ref. [1]), which depicts a comparison of the curves $K = K(G/b)$ for a biplane without winglets, for the corresponding box–wing body, and for a biplane with winglets (winglet length $0.4c$, where c is the root chord).

It should be observed that the above results have been obtained using a prescribed–wake approach, in order to be consistent with the Prandtl model which is based on the lifting–line theory. However, the present methodology is able to capture the effects of the wake roll–up on the airloads by using a free–wake approach, as described above. Figure 4 (also from Ref. [1]) depicts the Prandtl factor K as a function of G/b, for free–wake and prescribed–wake analysis. The results obtained by a free–wake approach show that the wake roll–up effect is to reduce the value of K. For the range of G/b of practical interest in aeronautical applications (*i.e.*, $0.1 < G/b < 0.2$), we have that the reduction of K is about 6% for the case of a box–wing. This demonstrates the importance of including a rolled–up wake in the analysis.

Next, consider new potential–flow results obtained with the formulation of Ref. [1]. In particular, Fig. 5 present a parametric study of the effects of the sweep angle (of the front and rear wing) on the Prandtl factor K of the Prandtl–plane shown in Figures 1 and 2. Here, we have considered three different configurations characterized by: (a) Mid–chord front wing sweep angle $\Lambda_F = 35°$ and mid–chord rear wing sweep angle $\Lambda_R = -40°$, (b) mid–chord front wing sweep angle $\Lambda_F = 37°$ and mid–chord rear wing sweep angle $\Lambda_R = -37°$ and, (c) mid–chord front wing sweep angle $\Lambda_F = 40°$ and mid–chord rear wing sweep angle $\Lambda_R = -35°$. We can note that the Prandtl factor of all three configuration are hardly distinguishable,

and are very close to the value of the Prandtl factor of the Best Wing System (continuous line). This is very important because it shows that, even for the Prandtl–plane, we have a reduction of induced drag, with respect to a traditional wing configuration.

Next, consider some preliminary results for attached high–Reynolds viscous flows. The two–dimensional integral boundary–layer formulation, used a 'strip–theory' in three-dimensional application, has been validated in Ref. [1], by comparison with experimental results available in literature, in the case of: *(i)* isolated wing, *(ii)* biplane, and *(iii)* box–wing configuration. For the sake of completeness the results for the third case are presented here in Fig. 6 (also from Ref. [1]) which depicts the polar at $Re = 5.1 \cdot 10^5$ of a box–wing configuration with aspect ratio 5, gap $G = c$, stagger $S = c$ and section profiles NACA 0012. The numerical results are in good agreement, also in this case, with the experimental results by Gall and Smith [6]. Next consider new results. The formulation of Ref. [1] has been used for a parametric study of the effect of sweep angle on the polar of a Prandtl–plane. This is shown in Fig. 7 which depicts a polar for the same three configuration of Prandtl–plane used in Fig. 5. We can note that their difference is very small.

Next consider the validation of third–order formulation. Some results have been presented in Morino and Bernardini [21] for the case of simply (RAE wing) and multiply connected (nacelle) configurations. Here, we consider the particularly challanging case of a wing with strake (see Fig. 8), at angle of attack $\alpha = 5°$ and having symmetric NACA 0002 airfoil sections. Fig. 9 depicts the circulation $\Gamma = \Delta\varphi_{TE}$ as a function of $2y/b$, while Fig. 10 shows the chordwise distribution of the pressure coefficient (at $2y/b = .219$). The present results are obtained with a chordwise discretization $N_1 = 20$ and a spanwise discretization $N_2 = 12$, and are compared with those obtained with the method of Roberts and Rundle [26] with $N_1 = 39$ and $N_2 = 24$ and those obtained with the method of Rubbert and Saaris [27] with $N_1 = 28$ and $N_2 = 12$. The agreement among the three formulations is good, except at the trailing–edge, where the pressure predicted in our case is higher (see also Ref. [21] which shows why our results appear to be more reliable).

Finally, we present some preliminary results of the three–dimensional boundary layer formulation. In particular, Figs. 11 and 12 show respectively the chordwise distribution (at $\eta = 0.5$ and for the upper surface of the wing) of the streamwise displacement thickness, δ_1^*, and the shape factor, H, for a RAE wing with mid–chord sweep angle $\Lambda = 45°$, RAE 101 airfoil secton at $Re = 2.1 \cdot 10^6$ and angle of attack $\alpha = 6.3°$. Our numerical results, obtained using $N_1 = 60$ and $N_2 = 10$, have been compared with the numerical results of Milewski [15] (obtained using $N_1 = 64$ and $N_2 = 10$), and experimental results of Brebner and Wyatt [2]. The transition location, in this case, is fixed using experimental data. We have also included in the figure the two–dimensional boundary layer formulation (unfortunately with transition obtained by Michel method [14]). Our three–dimensional numerical results are in good agreement with both the Milewski [15] and with experimental data. On the contrary, the 2D formulation shows, at the trailing edge, a great difference. This could find a justification in the fact that, at the trailing edge, the 3D effects are higher.

To conclude the paper we wish to mention a technique that allows us to overcome the boundary layer limitations. This is based on a decomposition introduced by Morino [17] for the velocity field as $\mathbf{v} = \nabla\varphi + \mathbf{w}$, where $\mathbf{w}$ (obtained by direct integration of $\nabla \times \mathbf{w} = \boldsymbol{\zeta} := \nabla \times \mathbf{v}$) has the property that $\mathbf{w} = 0$ where $\boldsymbol{\zeta} = 0$. This decomposition has been successfully applied to 2D steady full potential flows with boundary–layer correction (see Morino *et al.* [19]) and to 2D steady Euler flows, obtained as an exact correction to the full–potential solver (see Iemma *et*

al. [10]). The coupling of Euler with the boundary layer is now under investigation.

References

[1] Bernardini, G., Frediani, A., and Morino, L., "MDO of an Innovative Configuration - Aerodynamic Issues," Proceedings of the International Forum on Aeroelasticity and Structural Dynamics, Williamsburg 1999.

[2] Brebner, G.G., Wyatt, L.A., "Boundary Layer Mesurements at Low Speed on Two Wings of 45° and 55° Sweep," CP 544, Aeronautical Research Council, 1961.

[3] Drela,M.,"XFOIL: An Analysis and Design System for Low Reynolds Number Airfoils," in T.J. Mueller, editor, *Low Reynolds Number Aerodynamics,* 1989.

[4] Frediani, A., Chiarelli, M., Longhi, A., D'Alessandro, C.M., Lombardi, G., "Structural Design and Optimization of the Lifting System of a Non–Conventional New Large Aircraft," Proceedings of the CEAS International Forum on Aeroelasticity and Structural Dynamics, Rome 1997.

[5] Frediani, A., Lombardi, G., Chiarelli, M., Longhi, A., D'Alessandro, C.M., Bernardini, G., "Proposal for a New Large Airliner with a Non-Conventional Configuration," Proceedings of the XIV AIDAA Congress, Naples, 1997.

[6] Gall, P.D. and Smith, H.C., "Aerodynamic Characteristics of Biplanes with Winglets," *J. Aircraft,* Vol. 24, No. 8, pp. 518-522, 1987.

[7] Gennaretti, M., Salvatore, F., Morino, L., "Forces and Moments in Incompressible Quasi-Potential Flows," *Journal of Fluids and Structures,* Vol. 10, pp. 281-303, 1996.

[8] Gennaretti, M., Calcagno G., Zamboni A. and Morino L., 'A high order boundary element formulation for potential incompressible aerodynamics,' *The Aeronautical Journal,* Vol. 102, No. 1014, p. 211-219, 1998.

[9] Green, J.E., Weeks, D.J., Brooman, J.W.F., "Prediction of Turbolent Boundary Layers and Wakes in Compressible Flow by a Lag-Entrainment Method," RAE RM 3791, 1973.

[10] Iemma, U., Marchese, V., Morino, L., "Euler Flows Via BEM: a Potential/Vorticity Integral Formulation," Proceedings of ICES Conference, Atlanta, USA, 1998.

[11] Johnston, J.P.,"On the Three-Dimensional Turbulent Boundary Layer Generated by Secondary Flow," *J. of Basic Engineering,* Series D, Vol. 82, pp. 233-248, 1960.

[12] Lighthill, M.J., "On Displacement Thickness," *J. Fluid Mech.,* Vol. 4, pp. 383-392, 1958.

[13] Mangler, K.W., Smith J.H.B., (1970) Behaviour of the vortex sheet at the trailing edge of a lifting wing, *The Aeronautical Journal,* Vol. 74, pp. 906-908.

[14] Michel, R., "Etude de la Transition sur les Profils d'Aile–Establissement d'un Point de Transition et Calcul de la Trainée de Profil en Incompressibile," ONERA Rep. No. 1/1578A, 1952.

[15] Milewski, W.M.,"Three-Dimensional Viscous Flow Computations Using the Integral Boundary Layer Equations Simultaneously Coupled with Low Order Panel method," PhD Thesis, Department of Ocean Engineering, Massachsetts Insitute of Technology, 1987.

[16] Morino, L., "A General Theory of Unsteady Compressible Potential Aerodynamics," NASA CR-2464, 1974.

[17] Morino, L., "Helmholtz and Poincaré Velocity–Potential Decomposition for the Analysis of Unsteady Compressible Viscous Flows," in: Banerjee, P.K., and Morino, L., (Eds.): *Boundary Element Methods in Nonlinear Fluid Dynamics.* Elsevier Applied Science Publishers, London, 1990.

[18] Morino, L., "Boundary Integral Equation in Aerodynamics," *Appl. Mech. Rev.,* Vol. 46, August 1993.

[19] Morino, L., Gennaretti, M., Iemma, U., Salvatore, F., "Aerodynamic and Aeroacoustics of Wings and Rotors via BEM - Unsteady, Transonici, and Viscous Effects," *Comp. Mech.,* N. 21, 1998.

[20] Morino, L., and Bernardini, G., "Singularities in Discretized BIE's for Laplace's Equation; Trailing-Edge Conditions in Aerodynamics," Wendland, W.L., (ed.): *Mathematical Aspects of Boundary Element Methods*, CRC Press, London, UK, (in print).

[21] Morino, L., Bernardini, G., "Recent Developments on a Boundary Element Method in Aerodynamics," IUTAM Symposium on Advanced Mathematical and Computational Mechanics Aspects of the Boundary Element Method, Cracow, 1999.

[22] Mughal, B.H.,'A Calculation Method for Three-Dimensional Boundary-Layer Equations in Integral Form,' Master's Thesis, Department of Aeronautics and Astronautics, Massachusetts Institute of Technology, 1992.

[23] Nenadovitch, M., "Recherches sur les Cellules Biplanes Rigides d'Envergue Infinie," Publications Scientifiques et Techniques du Ministere de L'Air, Institute Aerotechnique de Saint-Cry, Paris, 1936.

[24] Nishida, B.A.,'Fully Simultaneous Coupling of the Full Potential Equation and the Integral Bounday Layer Equations in Three Dimentions,' PhD Thesis, Department of Aeronautics and Astronautics, Massachsetts Insitute of Technology, 1986.

[25] Prandtl, L., "Induced Drag of Multiplanes," NACA TN 182, 1924.

[26] Roberts, A., and Rundle, K., "Computation of incompressible flow about bodies and thick wings using the spline–mode system," BAC(CAD) Report Aero Ma 19, 1972.

[27] Rubbert, P.E., and Saaris, G.R., "Review and Evaluation of a 3-D Lifting Potential Flow Analysis Method for Arbitrary Configurations," AIAA Paper 72 - 188, 1972.

[28] Squire, H.B. and Young, A.D., "The Calculation of the Profile Drag of Airfoils," ARC RM No. 1838, 1938.

[29] Suciu, E.O., and Morino, L., "Nonlinear Steady Incompressibile Lifting-Surface Analysis with Wake Roll-Up," AIAA Journal, Vol. 15, No. 1, pp. 54-58, 1976.

[30] Thwaites, B., "Approximate Calculation of the Laminar Boundary Layer," *Aeron. Quart.* Vol. 1, pp. 245-280, 1949.

[31] Trefftz, E., "Prandtlsche Tragflächen und Propeller Theorie," Zeitschrift für Angewandte Mathematik und Mechanik, 1, Berlin, 1921.

[32] Wolkovitch, J., "The Joined Wing: An Overview," *J. Aircraft,* Vol. 23, pp. 161-178, 1986.

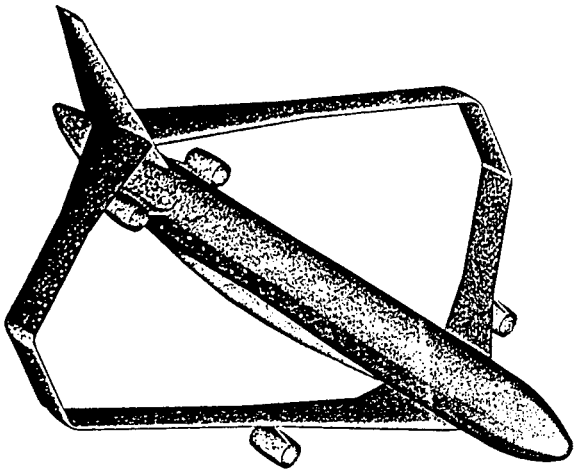

Fig. 1. Isometric view of Prandtl–plane.

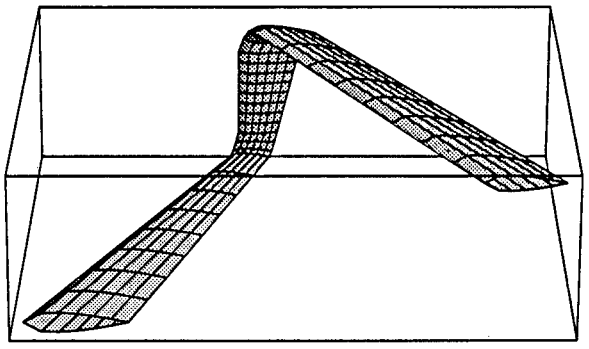

Fig. 2. Isometric view of wing of Prandtl–plane.

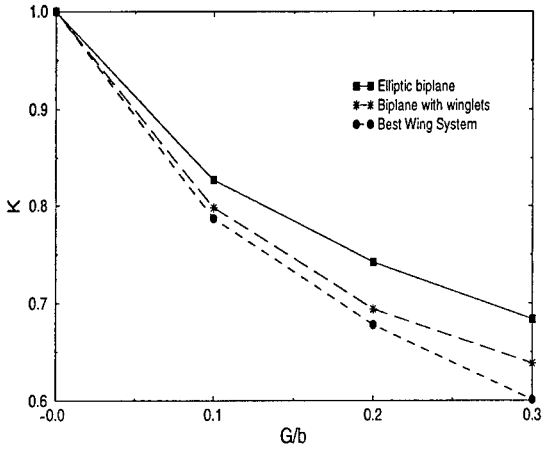

Fig. 3. Effect of winglets on Prandtl factor: rectangular biplane ($b/c = 10$, $\alpha = 5°$, unstaggered).

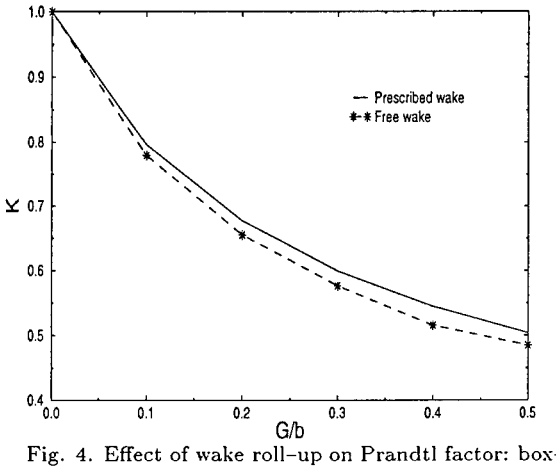

Fig. 4. Effect of wake roll-up on Prandtl factor: box–wing body ($b/c = 10$, $\alpha = 5°$, unstaggered).

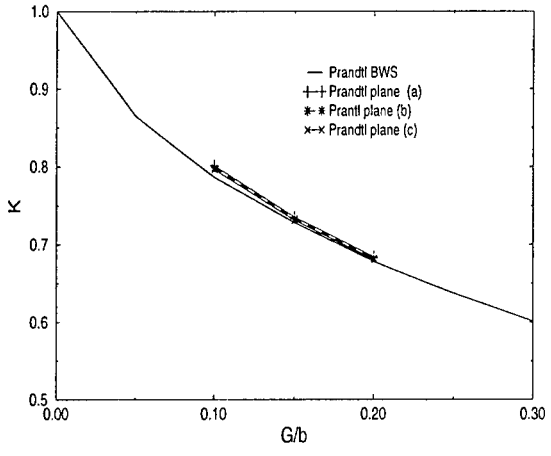

Fig. 5. Effect of sweep angle on Prandtl factor: Prandtl–plane.

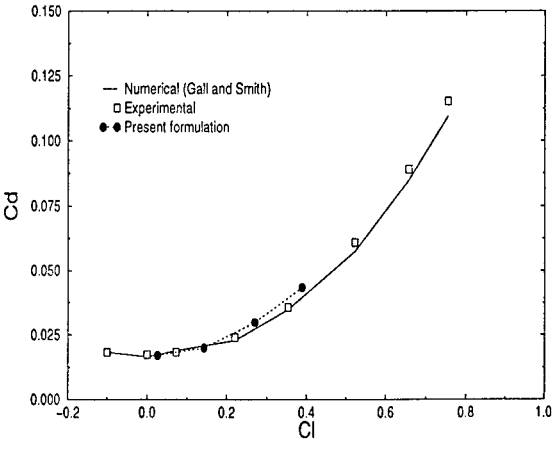

Fig. 6. Polar of box–wing body (aspect ratio 5, $G/c = 1$, stagger $= c$, section: NACA 0012) at $Re = 5.1 \cdot 10^5$.

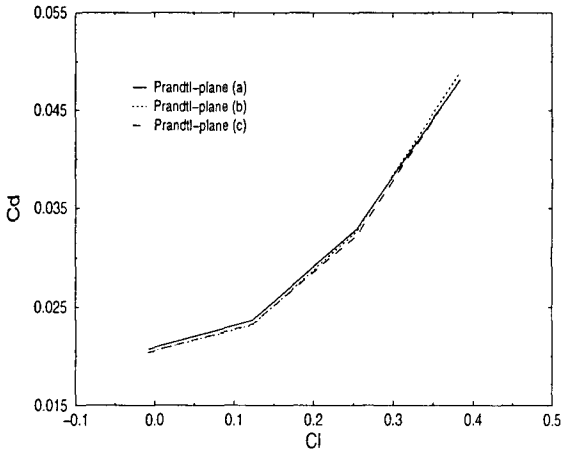

Fig. 7. Effect of sweep angle on polar of a Prandtl–plane at $Re = 2.7 \cdot 10^6$.

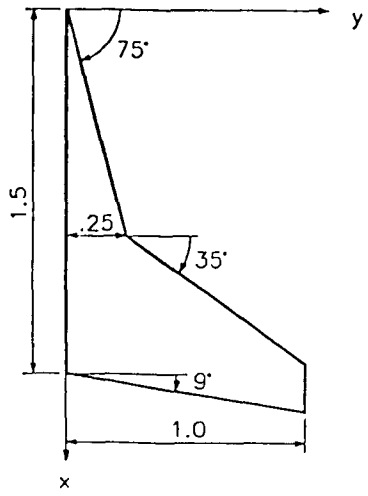

Fig. 8. Planform of wing with strake

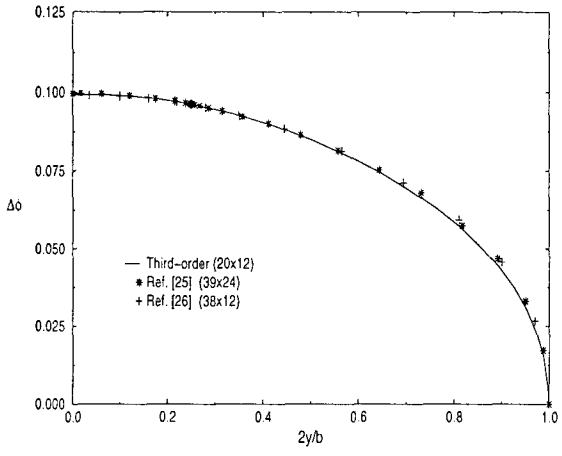

Fig. 9. Spanwise distribution of the circulation, $\alpha = 5°$.

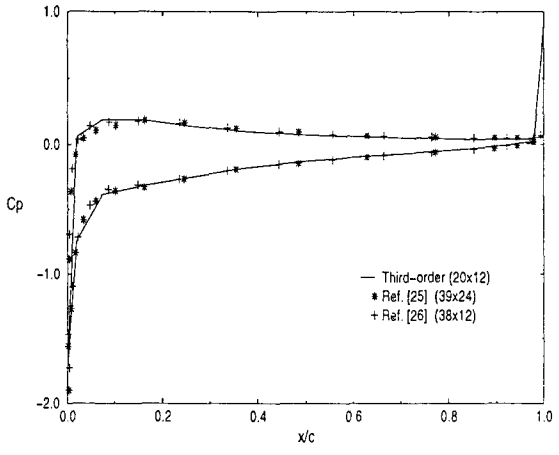

Fig. 10. Chordwise distribution of the C_p, $\alpha = 5°, \eta = 0.219$.

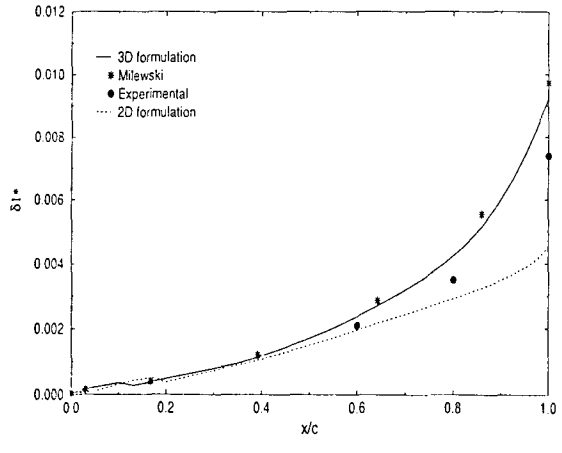

Fig. 11. Chordwise distribution of δ^*_1 at $Re = 2.1 \cdot 10^6$, $\alpha = 6.3°$, $2y/b = 0.5$.

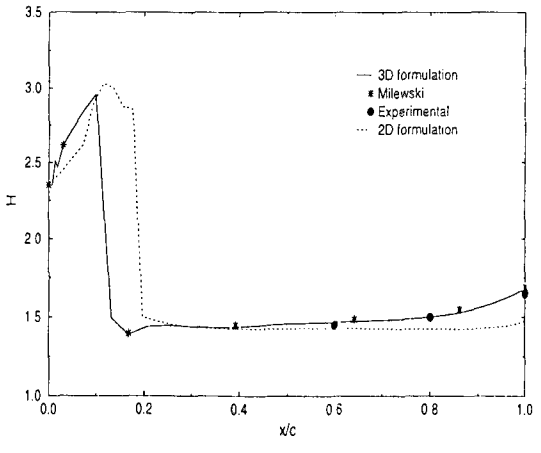

Fig. 12. Chordwise distribution of shape factor H at $Re = 2.1 \cdot 10^6$, $\alpha = 6.3°$, $2y/b = 0.5$.

DISCUSSION

Session II, Paper #16

Herr Sacher (DASA, Germany) asked how the engine would be represented in the potential approach.

Prof Morino noted that in the past, the engine has been represented by a prescribed flow at the inlet with a rigid surface. As this rigid surface should be coincident with the actual stream surface, iteration is required to determine this shape. In this present work, the approach is to model the jet with a prescribed uniform flow plus a wake (doublet layer) to model the velocity discontinuity between the jet and the surrounding flow. It was noted that this would be an ideal application of the viscous flow extension discussed during the presentation.